Mon. Not. R. Astron. Soc. **347,** 1241–1254 (2004)

Relation of radio-quiet quasars to galaxy clusters at $z < 0.3$

Ilona K. Söchting,[1,2★] Roger G. Clowes[3] and Luis E. Campusano[4]

[1]*Isaac Newton Group, Apartado de Correos 321, 38700 Santa Cruz de La Palma, Canary Islands, Spain*
[2]*Centre for Astrophysics, University of Central Lancashire, Preston PR1 2HE*
[3]*Computational Astrophysics, Department of Computing, University of Central Lancashire, Preston PR1 2HE*
[4]*Observatorio Astronómico Cerro Calán, Departamento de Astronomía, Universidad de Chile, Casilla 36-D, Santiago, Chile*

Accepted 2003 October 16. Received 2003 October 10; in original form 2003 January 24

ABSTRACT

We investigate whether radio-quiet quasars (RQQs) with $z < 0.3$ (and predominantly of low luminosity) are located preferentially in specific regions with respect to the centres and boundaries of neighbouring galaxy clusters. This way of characterizing the environment of RQQs differs from previous studies, which relied on the galaxy excess statistics within small radii around the quasars. For the detection of galaxy clusters we use a robust, semiparametric method based on a maximum likelihood estimate applied to Voronoi tessellation and enhanced by a colour-cut approach, allowing boundary determination and redshift estimates. We find that most of the RQQs reside within 3 h^{-1} Mpc of the centre of a galaxy cluster with comparable redshift and that none of them lies in the core itself. About 20 per cent of the investigated quasars reside between two galaxy clusters, which are possibly at an early stage of merger. Consequently, we suggest that quasars found in rich environments are associated with cluster mergers whereas those found in poorer environments are associated with infall towards a cluster. The information on larger scales provided by our analysis thus allows a clearer interpretation of the diverse environments that have for many years been reported in the literature for smaller scales. We discuss our findings in the context of existing quasar formation models and suggest that at least two formation mechanisms coexist. Additionally, we confirm, using multiple data sets, that low-redshift quasars follow a narrow channel of width $\sim$10 h^{-1} Mpc around the large-scale structure (LSS) traced by galaxy clusters, in agreement with the first report of this effect by Söchting, Clowes & Campusano. Such a result, if it applies to quasars at higher redshifts, has the potential to explain the clustering of quasars on scales $<$10 h^{-1} Mpc found initially by Shanks et al. The association of the LSS in clusters with the spatial distribution of quasars is not reproduced by samples of narrow emission-line galaxies (NELGs), indicating that the occurrence of NELGs does not require the same environmental conditions as that of quasars.

Key words: galaxies: clusters: general – quasars: general – cosmology: large-scale structure of Universe.

1 INTRODUCTION

Quasars were recognized as probes of the quasi-linear regime of hierarchical theories of structure formation within the cold dark matter (CDM) scenario over a decade ago (Efstathiou & Rees 1988). Although current models are better tuned to the observations than the early ones, they cannot be discriminated effectively through quasar counts and spatial distributions without a better understanding of how quasars trace the underlying mass distribution. The host galaxy mass function, quasar lifetime and occurrence probability are factors that can be illuminated through studies of the environments of quasars on scales ranging from the host galaxy to even the large-scale structure (LSS) in the galaxy distribution.

The emerging picture is that radio-loud quasars (RLQs) have elliptical host galaxies whereas radio-quiet quasars (RQQs) have elliptical and spiral host galaxies (e.g. Bahcall et al. 1997; Boyce et al. 1998) with the brightest ones ($M_R \lesssim -24$) residing in massive ellipticals (McLure et al. 1999). In many cases the host galaxies show traces of continuing interactions or past mergers (e.g. Bahcall et al. 1997; Boyce et al. 1998; Hutchings et al. 1999). Some of the host galaxies, which in the optical passband appear to be isolated and apparently undisturbed, are found to exhibit continuing or remnant

★E-mail: iks@ing.iac.es

tidal H I disruptions, indicating past galactic encounters or mergers (Lim & Ho 1999).

Investigations of galaxy counts or the quasar–galaxy covariance function within small radii (usually $< 1\ h^{-1}$ Mpc) around quasars indicate that RQQs and RLQs can be associated with structures ranging from poor groups to rich clusters of galaxies (Crampton, Cowley & Hartwick 1989; Saxton, Hall & Turner 1999; Wold et al. 2001; Hutchings et al. 1999; Teplitz, McLean & Malkan 1999; Sánchez & Gomzáles-Serrano 1999). Although some authors have found in the past that RLQs are found in richer surroundings than RQQs (Yee & Green 1987; Ellingson, Yee & Green 1991), more recent studies find a similar range of environments (McLure & Dunlop 2001).

On the scales of superclusters ($\sim 60\ h^{-1}$ Mpc) low-redshift RQQs follow the LSS traced by galaxy clusters (Söchting, Clowes & Campusano 2002), but they avoid the central density peaks of the clusters (e.g. Robertson 1983; Yee 1992; Söchting et al. 2002). Söchting, Clowes & Campusano (2001) have suggested that RQQs found in the richest environments are actually between two merging clusters, and the others tend to occupy the peripheries of clusters. These results motivated us to investigate the relative probability of quasar formation as a function of environment. While the richness measures based solely on galaxy counts provide a fast means of tabulating and comparing results within large data sets, they do not allow any consideration of the morphology of the distribution. In contrast to the existing studies we aim to determine what physical structures in the galaxy distribution are associated with quasars. The results presented in this paper have been obtained from the analysis of a large sample of low-redshift ($z < 0.3$), low-luminosity quasars (including Seyferts), based on semiparametric and fully automated methods, which provide statistically consistent and physically significant results and which exclude any subjective bias.

In the next section we describe the selection of the quasar sample and the data used to investigate the associated galaxy distribution. In Section 3 we provide a detailed account of the cluster detection method we have developed for this project and we summarize the procedure used to delineate the LSS. The properties of the cluster sample are described in Section 4. Section 5 contains the results of our investigation into how quasars trace the LSS and whether narrow emission-line galaxies (NELGs) follow a similar pattern. The relation of quasars to neighbouring galaxy clusters is investigated in Section 6. The discussion and conclusions concentrate on the constraints our results put on the existing quasar formation models, and are contained in Section 7. We have adopted the Einstein–de Sitter cosmological model with $H_0 = 100\,h$ km s^{-1} Mpc^{-1} and $h = 0.7$.

2 DATA

The goals of our investigation demand sampling of the galaxy distribution at least on the scale of superclusters, which requires very wide coverage at low redshift ($60\ h^{-1}$ Mpc or $\sim 6^\circ$ at $z = 0.3$) or very high depth with medium coverage at intermediate redshifts ($V \sim 25$ and $\sim 2^\circ$ at $z \sim 0.6$). Currently, only the low redshifts are accessible from public wide-field multicolour imaging surveys, e.g. the United Kingdom Schmidt Telescope (UKST) and the Palomar Observatory Sky Survey (POSS). The selection of the appropriate quasar sample proved to be a difficult task, because most surveys contain only a few low-z quasars.

We have selected four fields with areas ranging from ~ 27 to ~ 56 deg^2 (see Table 1 for details), and overall containing 60 quasars and Seyferts (S1, S2) spanning the redshift range $0.1 < z < 0.3$ and luminosity $-19.5 \gtrsim M_V \gtrsim -24.5$ (Fig. 1). All of these objects have been drawn from the Quasars and Active Galactic Nuclei (10th edn) Catalogue (Véron-Cetty & Véron 2001).

Table 1. Details of the fields of investigation. RA and Dec. are reference coordinates of the field position; N_q is the number of quasars in the redshift range $0.1 < z < 0.3$.

Field	RA (J2000) (h: m: s)	Dec. (J2000) (°: ′: ″)	Area (deg^2)	N_q	N_q/deg^2
1	10:05:30	−00:30:00	56	18	0.32
2	00:23:00	−29:30:00	27	12	0.44
3	21:31:00	−44:30:30	30	14	0.47
4	02:54:00	+00:30:00	36	16	0.44

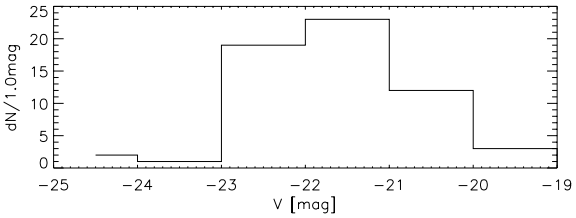

Figure 1. The luminosity distribution of the quasar sample.

Objects for the determination of the density distribution have been drawn from the SuperCosmos Sky Survey (SSS; Hambly et al. 2001). To reduce differences between the fields caused by the varying depth of the data, the limiting magnitude of the poorest plates has been imposed (21.00 and 22.65 mag in R and B_J, respectively) on all fields.

Star–galaxy separation is very unreliable beyond $B_J = 20.5$ mag (Hambly et al. 2001). To ensure that the population of faint cluster galaxies will be included in the data, we have removed only objects classified as stars which are brighter than $B_J = 20.0$ mag. The remaining star contamination is assumed to form a uniform background (Söchting et al. 2002). The removal of the brighter stars is very important, because they could lead to large errors in the cluster redshift estimates if included in a cluster colour–magnitude diagram.

3 CLUSTER DETECTION METHOD

We are interested in the exact position of quasars with respect to the cores of galaxy clusters – meaning the regions overpopulated by elliptical galaxies – and we want to resolve the subclusters if present. For these reasons, we need to preserve the morphological information when sampling the density distribution. Söchting et al. (2002) proposed Voronoi tessellation (VT) applied to colour slices for a similar application. We have enhanced our original method by introducing a maximum likelihood estimator (MLE) to better delineate the boundaries of the clusters. Allard & Fraley (1997) have described a non-parametric MLE using VT, which we have adapted for galaxy cluster detection.

VT provides a partition of a point pattern according to its spatial structure (see Fig. 2). The areas of the Voronoi cells can be used directly to determine the density distribution because $D_i = A_i^{-1}$, where D_i and A_i are respectively the density and the area of a cell corresponding to an object i. VT provides a non-parametric method of sampling of the underlying density distribution, which has been successfully used for finding galaxy clusters (Ramella et al. 2001; Kim et al. 2002; Söchting et al. 2001, 2002).

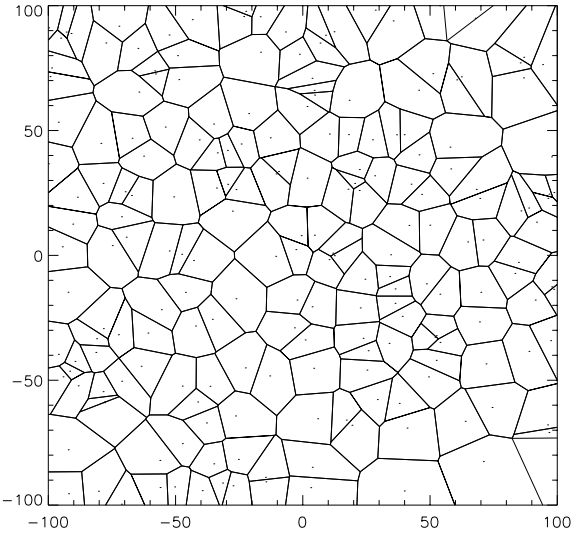

Figure 2. Example of VT. For more information on VT see Okabe et al. (2000) and references there.

Sampling of the density distribution is just the first step in a cluster detection procedure, followed by location of the density peaks that fulfil the criteria for a galaxy cluster (e.g. minimum number of member galaxies, colour or luminosity distribution). The simplest approach is to select objects with a certain contrast σ above the background. The contrast is defined as

$$\sigma_i = (\delta_i - \bar{\delta_{\rm b}})/\bar{\delta_{\rm b}},$$

making it most convenient to express the threshold contrast in terms of the mean background density $\bar{\delta_{\rm b}}$. We should remember that using Voronoi cells

$$\bar{\delta_{\rm b}} = \frac{1}{n}\sum_{i=1}^{n}\frac{1}{A_i}.$$

In the case of clusters with high contrast above the background, this approach produces very good results, and until now has been used in all VT-based procedures. The choice of the appropriate threshold brings a dilemma. With increasing threshold, the detection rate of the real clusters is declining, but also the relative number of spurious clusters detected is dropping. Moreover, in the outer regions of the clusters, where the number density is gradually dropping, the detection of the member galaxies is strongly dependent on the assumed threshold. Thresholding also introduces a bias towards clusters in regions of enhanced background, because it is not locally adaptive.

Most of these problems are overcome by introducing a MLE of the cluster galaxies. The MLE can be constructed by assuming the case of galaxies in a galaxy cluster as superimposed on 'noise' galaxies (i.e. foreground and background galaxies) producing a mixture of two random samples: (i) corresponding to the cluster and characterized by the probability p (the mixture parameter) and a support (area occupied by the cluster) $\mathcal{A} \subset K$, where K is the overall area of investigation; and (ii) corresponding to the background (plus foreground) with complementary probability $1 - p$ and support K. The mathematical framework presented below has been proposed by Allard & Fraley (1997).

The density associated with a point $x \in K$ is

$$f(x) = \frac{p}{|A|}\mathbf{1}_A(x) + 1 - p$$

where $\mathbf{1}_A = 1$ if $x \in \mathcal{A}$ and $\mathbf{1}_A = 0$ otherwise, and $|A|$ denotes the Lebesgue measure of $\mathcal{A}$ – normalized area in the two-dimensional case of the projected galaxy distribution with $|A|$ = physical area ($\mathcal{A}$)/physical area (K). The data-based likelihood of a sample of galaxies to be a cluster is

$$L(\boldsymbol{x}; \mathcal{A}, p) = \prod_{i=1}^{n}[f(\boldsymbol{x}_i)] = \left(\frac{p}{|A|} + 1 - p\right)^{N_A}(1-p)^{n-N_A}$$

where N_A is the number of objects in $\mathcal{A}$ and n is the number of objects in K. Because the mixture parameter p and $\mathcal{A}$ are not known, the above have to be reduced to a partial maximized (profile) likelihood. For a fixed $\mathcal{A}$, the MLE of p is

$$\hat{p} = (N_A - |A|n)/(n - |A|n)$$

and the partial maximized likelihood becomes

$$L(\boldsymbol{x}; \mathcal{A}) = \left(\frac{1}{n}\right)^{n}\left(\frac{N_A}{|A|}\right)^{N_A}\left(\frac{n-N_A}{1-|A|}\right)^{n-N_A}$$

and expressed as log-likelihood

$$l(\boldsymbol{x}; \mathcal{A}) = -n\ln n + N_A \ln\frac{N_A}{|A|} + (n - N_A)\ln\frac{n-N_A}{1-|A|}.$$

$\mathcal{A}$ is constructed from Voronoi cells ensuring that any constraints are defined by the data points themselves. The practical implementation of this method will be described in detail later in this section.

The disadvantage of the likelihood approach is its computing intensity. Without a pre-selection of possible cluster candidates this method would not be attractive at present because it loses all the speed advantages of the basic VT.

To accelerate the procedure, we have constructed a hybrid method, which uses thresholding in the preliminary step and MLE in the main process to reduce false detections and to improve the detection of the member galaxies in the outer regions of the clusters. The application of the MLE allows us to choose a rather low threshold, ensuring that the poor clusters in the regions of lower background density will be included. Too low a threshold, however, may result in the selection of only very few cluster candidates, because large areas corresponding to high background density and/or rich clusters will merge interconnecting real and spurious clusters and thus provide misleading input for the MLE algorithm. To remain consistent with the notation of the likelihood function, which has been defined in terms of the area of the Voronoi cells, we want to express the contrast of a cluster above background in terms of the area. If the density of the cluster galaxies is $\delta_{\rm cl}$ and that of the background galaxies $\bar{\delta_{\rm b}}$ than the contrast is

$$\sigma = \frac{(\delta_{\rm cl} + \bar{\delta_{\rm b}}) - \bar{\delta_{\rm b}}}{\bar{\delta_{\rm b}}} = \frac{\delta_{\rm cl}}{\bar{\delta_{\rm b}}}.$$

Because $\delta_{\rm cl} = N_A/\mathcal{A}$ and $\bar{\delta_{\rm b}} = (n - N_A)/K$ this becomes

$$\sigma = \frac{N_A}{\mathcal{A}}\frac{K}{n-N_A}.$$

Then, because $\mathcal{A}/K = |A|$, the contrast of a cluster is

$$\sigma = \frac{1}{n-N_A}\frac{N_A}{|A|}.$$

Assuming that the overall number of objects in the sample is very high compared with the number of cluster members, the size of an average Voronoi cell in a cluster is approximately

$$\langle|A_{\rm cl}|\rangle \approx \frac{1}{n\sigma}.$$

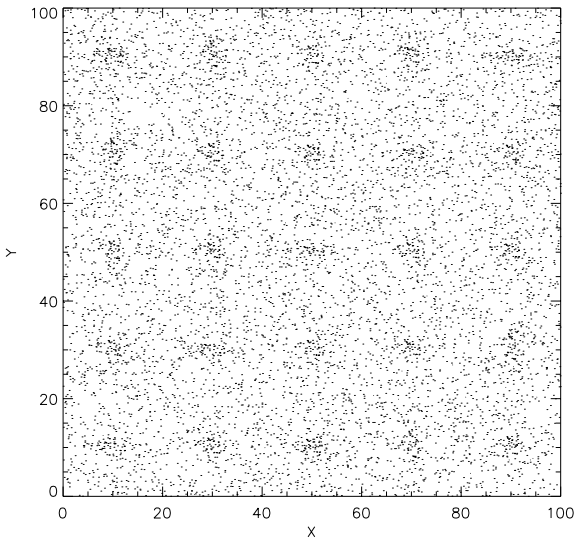

Figure 3. Example of 25 synthetic clusters with mean contrasts $\sigma = 6$ above the background as used to test the performance of the different density thresholds.

We need to remember that the cells in the cluster centre will usually be smaller due to higher central density and larger on the outskirts of the cluster where the density will be lower. The fluctuations of the background will introduce further uncertainties. We define the threshold as the lowest acceptable contrast and use it to calculate the maximum size of Voronoi cells to be selected as candidate cluster cells. For example, a threshold of 2.0 means that all cells satisfying $|A_i| = 1/(2.0\ n)$ are selected.

We have tested the lower range of the thresholds to find the lowest acceptable one which would achieve, in combination with the MLE, a very high detection rate with a low number of false detections. In the test, a synthetic set of 100 clusters was constructed, with a wide range of morphologies, expressed through rectangles with sides of varying ratios and different normal distributions in the x- and y-direction. The rectangles are of fixed area so that the mean density is constant for all clusters. Fig. 3 illustrates an example of 25 synthetic clusters with mean contrasts $\sigma = 6$ above the background.

The detection rate of these synthetic clusters and the relative contamination by spurious clusters have been investigated in the presence of a randomly distributed background. The performance of the hybrid-VT method with different thresholds has been compared by gradually increasing the background, to reduce the mean contrasts of the clusters from 16 to 4. Fig. 4 illustrates the performance of six thresholds (1.5, 1.7, 1.9, 2.1, 2.3 and 2.5) in a wide range of mean contrasts of the clusters over the background.

The best performance has been achieved by thresholds of 1.9 and 2.1 providing a detection rate of the synthetic clusters close to 1.0 with contamination by spurious clusters less than 30 per cent of the overall number of clusters detected. The detected boundaries of the clusters as compared to the original boundaries of the synthetic clusters are shown in Fig. 5 for the thresholds of 1.9 and 2.1 for clusters with mean contrasts $\sigma = 6$. We have selected the threshold of 2.0 for our application.

The use of colour slices has been proposed and tested by Gladders & Yee (2000). Selecting galaxies in colour slices in the colour–magnitude diagram increases the density contrast of any grouping of early-type galaxies, which are normally found in clusters or groups. A colour slice in the colour–magnitude plane provides separation in redshift space via the red sequence of early-type galaxies in clusters (Gladders & Yee 2000, and references inside), thus reducing considerably the projection effects.

The redshift range $0 < z < 0.4$ corresponds to a B_J–R colour space in the range $1.4 < B_J$–$R < 2.5$ using the E+S0 galaxy colours derived by Fukugita, Shimasaku & Ichikawa (1995). The limit in the redshift space for this pair of filters is $z \sim 0.4$, because the colours for higher-redshift ellipticals start to drop for $z > 0.6$, reaching B_J–$R \sim 2.5$ again at $z \sim 0.8$. Such high-redshift clusters are in any case beyond the magnitude limit of our data. Using the colours for the known clusters and the model predictions (Kodama et al. 1998) the initial estimate of the gradient of the slices in the colour–magnitude plane has been adopted as -0.05. The width of the slices is mainly dictated by the uncertainties in the photometric calibration and is empirically set to be $\Delta(B_J$–$R) = 0.2$ mag. The colour slices are overlapping in steps of 0.1 mag.

The procedure has been separated into two stages. In the first stage, we use thresholding of the Voronoi cells in colour slices giving us a set of cluster candidates with their preliminary members. Cluster candidates detected in different colour slices sharing three or more members are considered to be one cluster candidate (a derivative of the friend-of-friend algorithm). The colours and magnitudes of the preliminary members allow us to derive empirically the slopes and zero-points of the cluster red sequence in the B_J–R/R plane for every cluster candidate. In the second stage, for every cluster candidate the MLE algorithm is applied in a colour–magnitude slice described by width $\Delta m = 0.2$ mag and the slope and the zero-point determined in the first stage. The algorithm starts with the smallest cell of the preliminary members and includes all the adjacent cells which increase the likelihood. The procedure is repeated for their neighbouring cells until there are no adjacent cells to already selected ones which would further increase the likelihood. The galaxies found in the second stage to be cluster members are used to determine the final slope and the zero-point of the cluster red sequence, which are then used in redshift estimation. The boundary of the cluster is defined as the smallest convex-hull enclosing entirely the union of the Voronoi cells of the member objects. Only clusters with at least seven members are considered as real galaxy clusters and build the final sample. This minimum number of member galaxies has been set to separate poor groups from clusters. The process is entirely automated, excluding any subjectivity in the selection of clusters.

The colour–magnitude relation applies to the elliptical galaxies which are known to form the cores of the clusters. Strongly non-virialized clusters, such as Virgo, consisting of multiple subclusters, may be considered as associations of multiple separated cores.

There will be cluster members outside the 0.2-mag colour slice, especially towards the faint end of the magnitude axis. The technique described above should be considered as conservative, aiming to maximally reduce the number of false detections but at the expense of missing some of the population of the cluster galaxies. This has been dictated by the fact that a few false detections can strongly influence the reconstruction of the LSS.

4 CLUSTER SAMPLE

The application of the above procedure to the $\sim$150 deg^2 overall area of investigation produced a sample of 1021 galaxy clusters with estimated redshifts in the range $0.05 \leqslant z \leqslant 0.45$. The resulting density is 6.8 clusters deg^{-2} with $\langle z \rangle = 0.26$. The colour discrimination should make our sample mostly free of projection effects. As mentioned in the previous section, clusters with prominent substructure produce multiple detections with each subcluster being detected as a

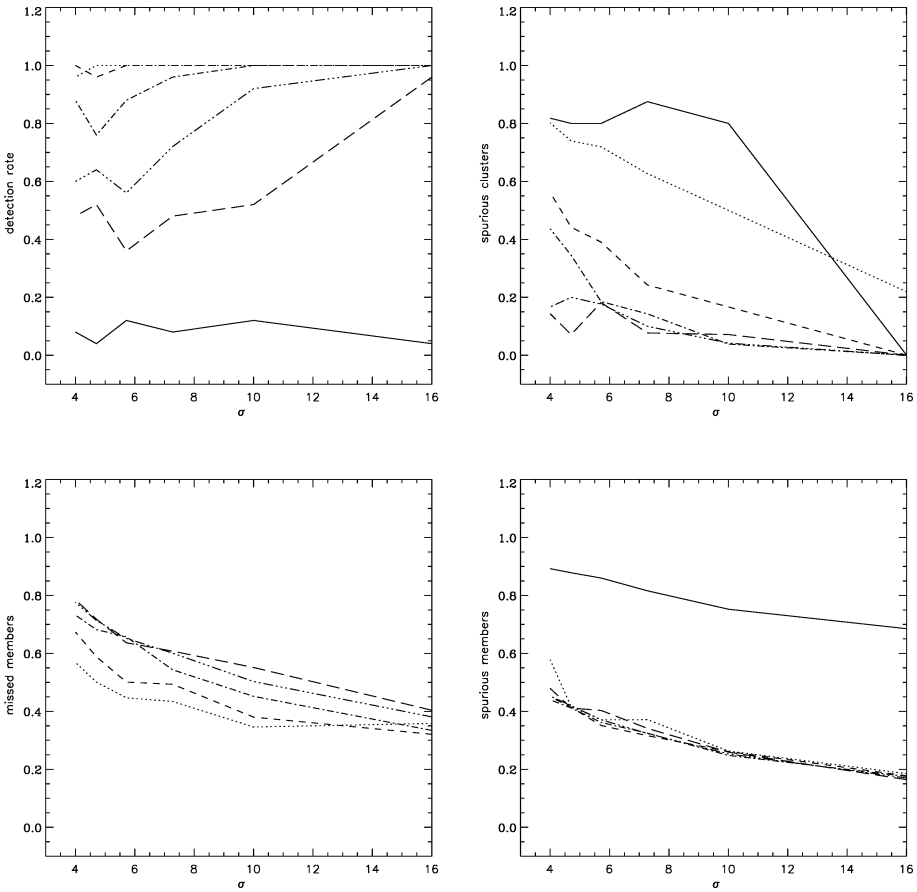

Figure 4. The performance of six thresholds (1.5, solid line; 1.7, dotted line; 1.9, dashed line; 2.1, dash-dotted line; 2.3, dash-triple-dotted line; 2.5, long-dashed line) in a wide range of contrasts σ of the clusters over the background.

separate cluster with its own red sequence. This feature is very important for the purpose of investigating quasar environments, because we can study quasar formation at the confluence of cluster/subcluster mergers. We estimate that about 30 per cent of the clusters found in this study are actually subclusters. The cluster statistics for the four fields of the investigation are given in Table 2.

Reference to the VizieR catalogue tool indicated that our areas contain 18 published galaxy clusters with spectroscopic redshifts. All of these have counterparts in our sample, allowing calibration into redshifts of the zero-points of the cluster red sequences. The number of calibration points per field is too low to determine the calibration field by field, but, because the SSS is colour-corrected, we have been able to construct a global calibration by combining the calibration points from all four fields. The polynomial fitted calibration curve (Fig. 6) follows the equation

$$z = -0.0449C_z^2 + 0.4626C_z - 0.5056$$

where C_z is the zero-point of the cluster red-sequence at $R = 17$. The uncertainty in the colour is $\delta(B_J–R) = 0.16$ mag (Hambly et al. 2001), which corresponds to an uncertainty in redshift of $\sim\pm 0.05$ at $z = 0.20$. There is a very large scatter in the colour–redshift relation at the lowest redshifts ($z < 0.1$); see Fig. 7. Because no quasars in our sample have redshifts lower than $z = 0.13$, we have excluded the lowest redshifts from our considerations and constructed a calibration starting at $z > 0.1$.

In our case the richness of the clusters is expressed by the number of red galaxies comprising the red sequence of the cluster. The richness distribution of the cluster sample (Fig. 8) indicates that most of the clusters have about 15 member galaxies. We should emphasize that only galaxies within 0.1 mag of the cluster red sequence have been considered, which usually excludes bluer spirals. The true richness of the clusters will therefore increase with increasing content of blue galaxies. A subsample of rich clusters, with at least 20 members, has been created to be used for the reconstruction of the LSS, as described in the next section. Assuming an average fraction of blue galaxies of $\sim(2/3)$, this subsample corresponds to Abell class $\gtrsim$0 galaxy clusters.

5 THE LARGE-SCALE ENVIRONMENT OF QUASARS

Söchting et al. (2002) have shown that low-redshift quasars trace the same LSSs as the galaxy clusters. This result was derived from an investigation of a single redshift slice ($z = 0.25 \pm 0.05$) in only one area of sky. The null hypothesis that the seven quasars were distributed independently of the LSS in clusters was rejected at a level of significance of 0.009. Here we further test this result using a larger set of quasars from the four fields (Table 1), and with the enhancement of the MLE in our technique.

In the four fields, the quasars have been separated into usable sets under two constraints: (i) the occupied redshift slice must not be wider than 0.1 ($\Delta z < 0.1$), to minimize projection effects; (ii) every usable set is required to have at least five members to avoid large errors. Using histograms of the redshift distribution (Fig. 9),

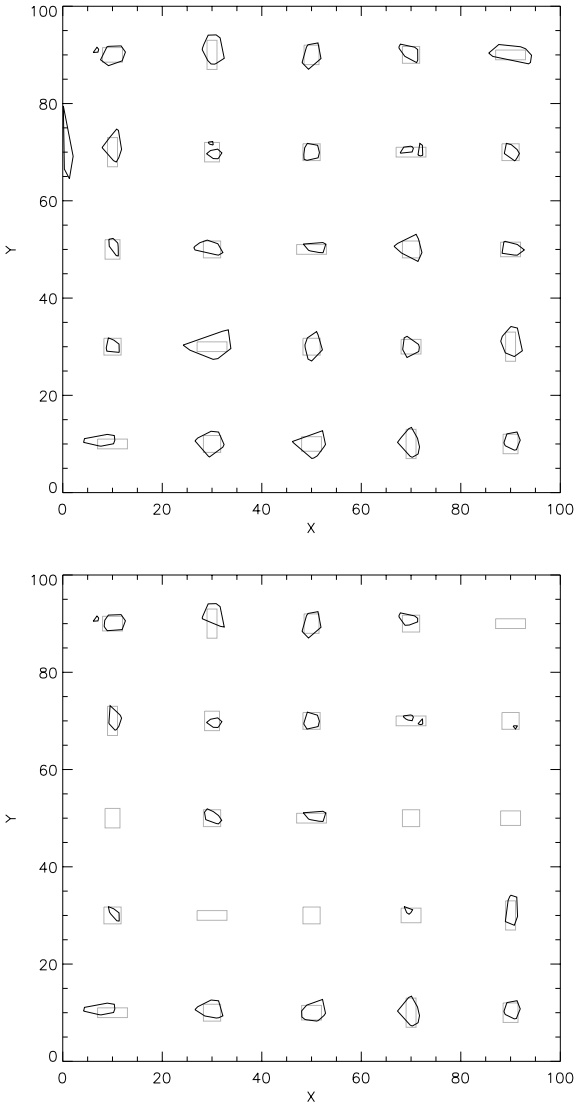

Figure 5. The detected boundaries of the clusters (black polygons) compared with the original boundaries of the synthetic clusters (grey rectangles) for the thresholds of 1.9 (top) and 2.1 (bottom) and a mean cluster contrast of 6.

six quasar sets totalling 51 objects have been selected, spanning, overall, the redshift range $0.13 < z < 0.3$. Table 3 contains the details for all the sets. The redshift range of the cluster sample has been selected to be always $\delta z = 0.04$ wider than the redshift range of the quasar sample to accommodate some of the redshift uncertainty while avoiding too large a range, which would introduce stronger projection effects.

The LSS is reconstructed using the rich galaxy clusters. The problem of connecting discrete objects into a continuous structure can be approached using another graph theoretical method, the minimal spanning tree (MST). This method has been successfully tested for finding large quasar groups (LQGs) in quasar samples (Graham 1997). The MST is a geometric construct, originating in graph theory, which was introduced by Kruskal (1956) and Prim (1957).

In our case the nodes of the MST are the galaxy clusters. For the purpose of this study we constructed two-dimensional MSTs. We did not attempt to separate the MSTs to recover the galaxy

Table 2. The statistics of galaxy clusters found in the four fields. RA and Dec. indicate the position of the field; N_c is the number of detected clusters in the field; d_c is the surface density of the clusters; $\langle z \rangle$ is the mean estimated redshift.

Field no.	RA (J2000) (^{h}: ^{m}: ^{s})	Dec. (J2000) ($^\circ$: $'$: $''$)	N_c	d_c (deg^{-2})	$\langle z \rangle$
1	10:05:30	−00:30:00	351	6.3	0.26
2	00:23:00	−29:30:00	203	7.5	0.25
3	21:31:00	−44:30:30	263	8.8	0.26
4	02:54:00	+00:30:00	204	5.7	0.25

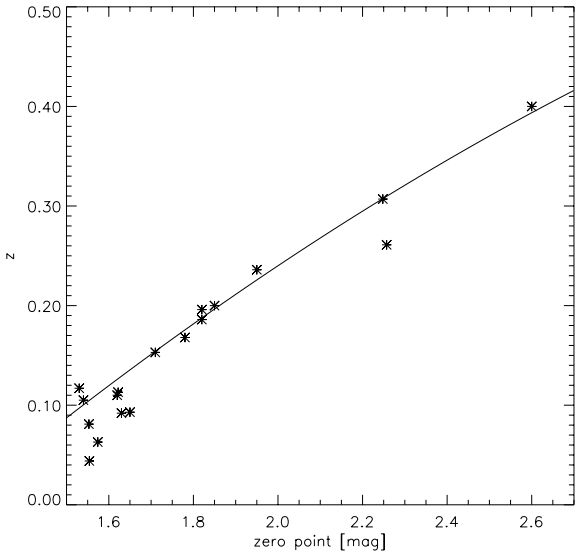

Figure 6. The calibration of the zero-points (defined at $R = 17$) into redshifts, using positionally matched published clusters found by the VizieR catalogue tool.

superclusters, but preserved the continuous LSS. As Fig. 10 shows, the quasars populate the region delineated by the MST as the LSS. To test the statistical significance of this result we resampled the quasar distribution using a Monte Carlo method. As a measure of how close the quasars follow the LSS, we have used the sum of the distances between quasars and their closest MST vectors $\sum_{i=1}^{n} r_i$. The results of 100 000 simulations are shown in Table 3. The test rejects the null hypothesis that the quasars are distributed independently of the LSS in clusters at a level of significance ranging from 0.074 for set number 4 to 0.003 for set number 5. Set number 4 has only five quasars, which is probably responsible for its apparently discrepant significance.

In some cases the quasar phenomenon has been linked with strong star formation (Evrard 1991). We could argue that, if both phenomena are environmentally connected, then quasars and star-forming galaxies may be expected to trace the LSS in a similar manner. The NELGs are usually assumed to be a mixture of low-luminosity active galactic nuclei (AGN) and starburst galaxies (Pearson et al. 1997). We have tested if the NELGs are such strong tracers of the LSS in galaxy clusters as quasars. Two fields of our study are contained within the 2dF Quasar Survey (Croom et al. 2001a) providing a well-defined sample of NELGs. Three sets of NELGs have been selected to cover the same areas and redshift ranges as the quasar sets in these two fields (Table 3). Applying the above analysis to

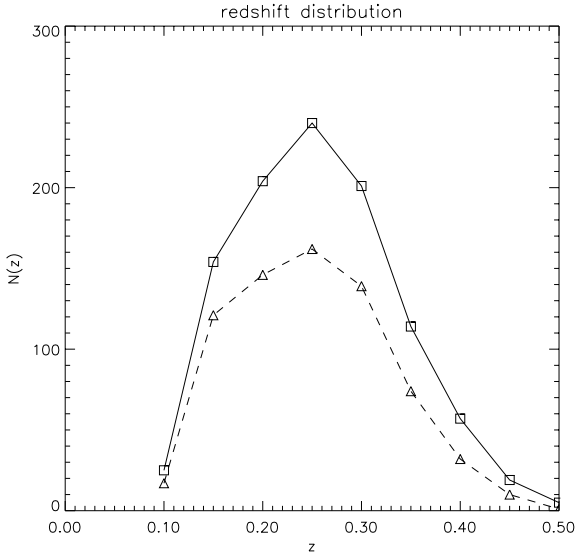

Figure 7. The redshift distribution of the detected clusters from the four fields (∼150 deg^2). The distribution of the whole sample is indicated by squares plus solid line, and that of the rich clusters (at least 20 members) by triangles plus dashed line.

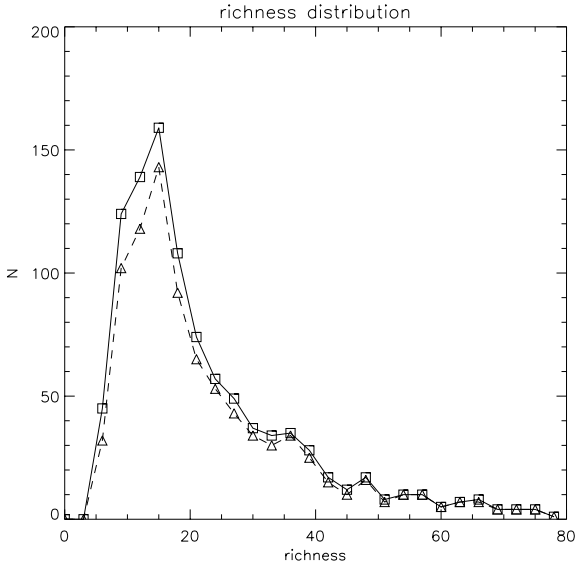

Figure 8. The richness distribution of the detected clusters. The distribution of the whole sample is indicated by squares plus solid line, and that of clusters with $0.11 < z < 0.32$ by triangles plus dashed line.

NELGs, we find that they are distributed at random with respect to the LSS, and appear to be unrelated to the quasars. From Fig. 10, some of the NELGs, nevertheless, inhabit very similar environments to those of the quasars and are even found in their vicinity.

6 THE SMALL-SCALE ENVIRONMENT OF QUASARS

The origin of the large variations in the richness of the environments of quasars has been investigated by studying the distribution of galaxy clusters within 5 h^{-1} Mpc radius at comparable redshift. The uncertainty in the cluster redshifts of $\delta z \sim 0.05$ means that a cluster redshift is considered as comparable to that of the quasar if it is within a redshift slice of width $\Delta z = 0.1$. We chose the projected distance from the quasar to the centre of the neighbouring cluster as a parameter to measure their connectivity, where the centre of a cluster is defined as the mean position of its members. In clusters that comprise multiple subclusters, every subcluster is treated as a separate entity with respect to the quasars.

In the investigated sample of 60 quasars, most of the quasars (28 objects, ∼47 per cent) reside within a projected distance of 1–3 h^{-1} Mpc from the cluster centre – on the peripheries of the clusters (see Fig. 11 for examples). Galaxy clusters are known to have radii from ∼0.6 to ∼2.5 h^{-1} Mpc (Girardi et al. 2000), suggesting that all of these quasars may indeed be associated with the adjacent clusters.

10 quasars (∼17 per cent) have been found to reside within 1 h^{-1} Mpc projected radius from a galaxy cluster centre (we refer later to these objects as residing in galaxy clusters), but none of them occupies the centre of the regions marked by the red galaxies forming the cluster red sequence. This result shows that even quasars inside a galaxy cluster are not located in its core but rather lie towards the cluster boundaries. Fig. 12 shows the relative position of the quasar having the smallest angular separation from the cluster centre and of the elliptical population marking the cluster core. The quasar redshift is $z = 0.299$ and the redshift of the galaxy cluster has been estimated as $z = 0.29$. This object is the only quasar found to reside within a galaxy cluster in which the host cluster does not exhibit any traces of continuing or past cluster mergers. Possibly this quasar is on the periphery of that cluster, but in the line of sight.

12 quasars (about 20 per cent of the sample) have been found between two close galaxy clusters/subclusters with comparable redshifts, suggesting that they could have formed at the confluence of merging clusters/subclusters (see Fig. 13 for examples). Most of these quasars are classified as residing in a galaxy cluster. Considering also the 10 quasars found in galaxy clusters ($d_{\rm proj} < 1\ h^{-1}$ Mpc), only three of them do not have an apparent merger companion. We cannot exclude that, in these three cases, the merging components are already too close to be detected as two clusters, or that merger is taking place in the line of sight. Two of the three clusters are very extended and the distribution of the red galaxies is discontinuous, suggesting multiple galaxy populations. In the third case the host cluster has a compact appearance and, as outlined before, the quasar could actually reside on the periphery of the cluster but in the line of sight. This behaviour suggests that essentially all quasars found in rich environments could have formed at the confluence of merging clusters.

There is a strong drop in the occurrence of quasars with more than 3 h^{-1} Mpc distance to the centre of the nearest cluster. The 22 quasars (∼36 per cent) found to lie at projected distance >3 h^{-1} Mpc to a cluster centre could possibly belong to a second population of RQQs not formed under the influence from galaxy clusters. They could, however, also be explained by incompleteness of the cluster sample. The cluster sample has been assessed to be complete to $z \sim 0.18$ and over 60 per cent complete at $z = 0.3$. None of the isolated quasars has $z < 0.19$ and their numbers increase with redshift. In the SSS the areas affected by the diffraction patterns from bright stars have been removed, leaving in many cases empty circles ∼15 arcmin across. Visual assessment of the regions around all quasars has shown that in many cases, where no close galaxy clusters have been found, multiple bright stars have been removed. We made one further test. In field number 4, there are four quasars occupying a small area (∼0.2 deg^2) without any close galaxy cluster being detected. The region is covered by the released data from the Sloan Digital Sky Survey (SDSS; Stoughton et al. 2002) providing us with data in the u', g', r', i' and z' passbands. The same cluster-finding routine has been applied to the g'–r' colour in the SDSS data, producing a list

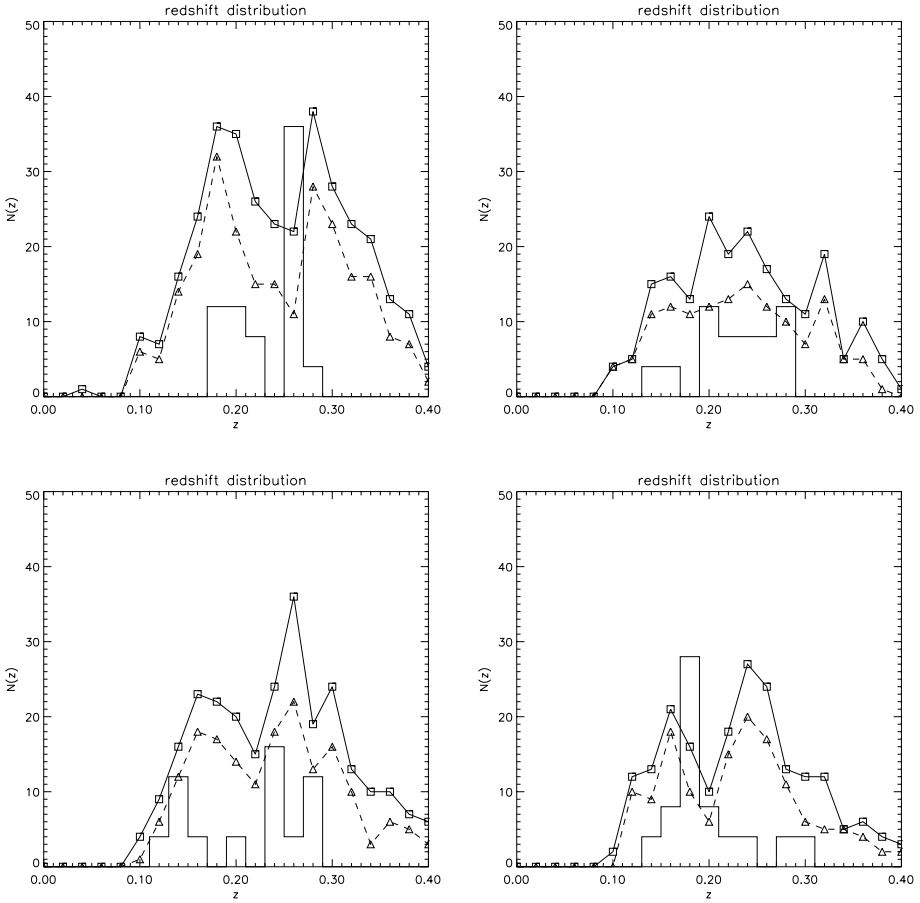

Figure 9. The redshift distribution of the quasars (bars) and galaxy clusters (squares plus solid line), with the rich clusters indicated by triangles plus dashed line. The $N(z)$ of the quasars has been multiplied by a factor of 4 to improve the clarity of the plot. The peaks in the quasar distribution are accompanied by enhancements in the cluster distribution. The small relative displacements of the peaks are within the errors for the redshifts of the galaxy clusters.

Table 3. The results for the six quasar sets selected to test the large-scale environment of quasars. Three of the sets have complementary NELG samples. The field numbers correspond to the rows in Table 1. N_q is the number of quasars in the set, and N_c is the number of galaxy clusters tracing the LSS in the corresponding redshift interval. P_q is the significance level at which the null hypothesis can be rejected that quasars are distributed independently of the LSS in clusters, and P_{NELG} is its counterpart for NELGs.

Set no.	Field no.	N_q	z range quasars	z range clusters	N_c	P_q	N_{NELG}	P_{NELG}
1	1	8	0.18–0.24	0.16–0.26	66	0.045	18	0.20
2	1	10	0.26–0.29	0.24–0.31	31	0.007	12	0.22
3	2	9	0.20–0.29	0.18–0.31	52	0.039	23	0.37
4	3	5	0.13–0.17	0.11–0.19	40	0.074	–	–
5	3	8	0.24–0.30	0.22–0.32	53	0.003	–	–
6	4	11	0.17–0.20	0.15–0.22	44	0.019	–	–

of four clusters in this region. Three of them are actually subclusters of the same cluster at estimated redshift $z \sim 0.20$ (the zero-point in g'–r' is 1.36 mag) which agrees very well with the redshift of three of the quasars ($z = 0.198$). The fourth cluster is at $z \sim 0.25$ (the zero-point is 1.70 mag), which is of similar redshift to the fourth quasar in this region ($z = 0.257$). The redshift calibration has been performed using the empirical colour limits and example clusters published by Kim et al. (2002).

We have tested for a luminosity dependence of our results, or dependence from the spectral classification (e.g. Seyfert 2s), but none has been found in (Fig. 14) the magnitude range $-23 < M_V < -19$. The three quasars with $M_V < -23$ have projected distances $<3\ h^{-1}$ Mpc, but no inferences can be drawn for this magnitude range.

7 DISCUSSION AND CONCLUSIONS

Quasars are potentially privileged objects for probing the cosmological models, because they are relatively easily detected in large numbers across a very wide range of redshifts. However, currently, quasar counts provide only very weak constraints on the cosmological models because of the limited understanding of the quasar formation mechanisms and evolution. The fundamental data in prompting models of quasar formation and fuelling are: (i) the dependence of the luminosity function on redshift; (ii) the quasar environment and its dependence on redshift and luminosity. The first of these is quite well specified, while the second, environment, can range from studies of the host galaxies to the superclusters where they lie. The emphasis in this paper is on the latter category, concentrating on the environment at the largest scales of clusters and superclusters. This approach, first suggested by Söchting et al. (2001), allows us to specify the quasar environment with respect to major density enhancements.

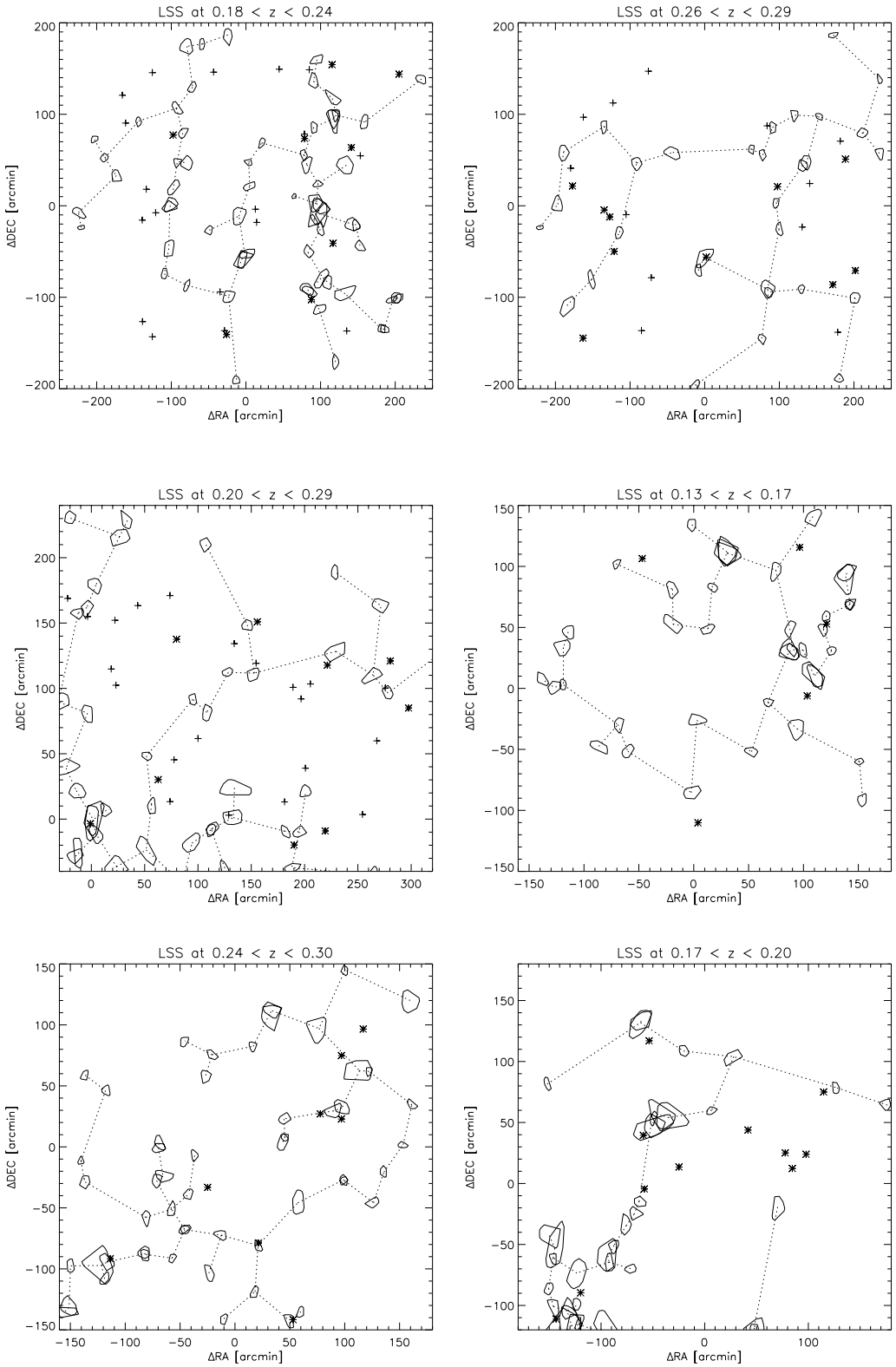

Figure 10. The relation between the LSS in galaxy clusters (polygons) delineated by the MST (dotted line) and quasars (asterisks) for the six sets as ordered from top-left to bottom-right. Three of the sets contain well-defined samples of NELGs (pluses). The axes correspond to X and Y in units of arcmin from the centre of the corresponding field.

Two principal groups of mechanisms have been proposed for the formation of quasars: (i) collapse of gas clouds, leading to the formation of a supermassive black hole and its fuelling; (ii) galaxy mergers and interactions, leading to the formation of a supermassive black hole from coalescence and its fuelling. The accumulated observational evidence, such as distorted morphologies of the host galaxies (Disney et al. 1995; Bahcall et al. 1997; Boyce et al. 1998; Hutchings et al. 1999), their large luminosities (Carballo et al. 1998) and

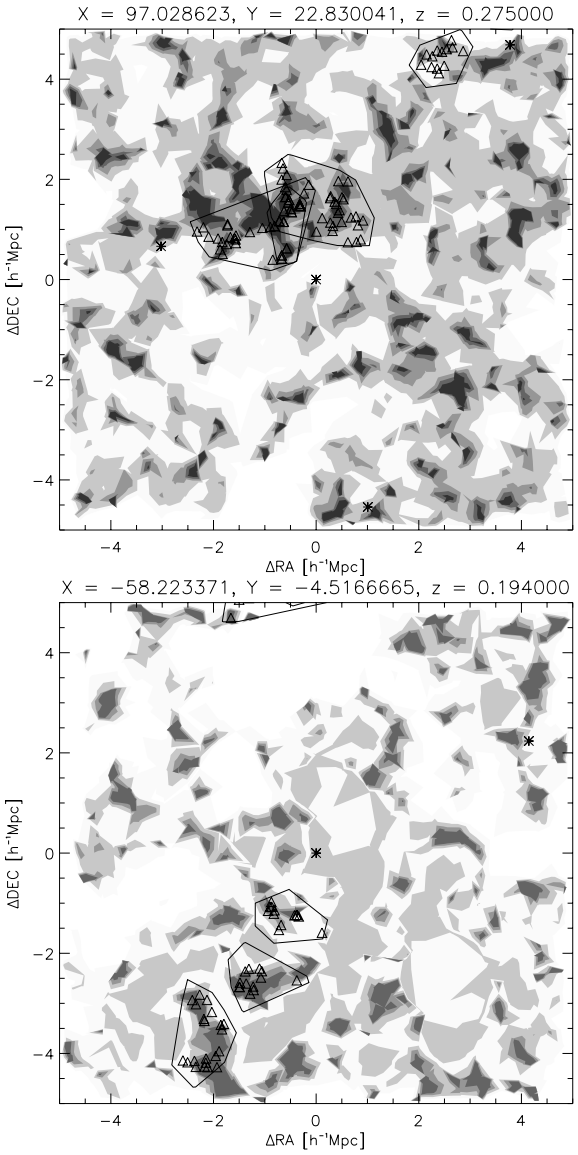

Figure 11. Two examples of quasars residing on the peripheries of galaxy clusters. The contours indicate the density of galaxies; the polygons outline the boundaries of galaxy clusters at comparable redshifts to those of the quasars (asterisks at coordinates 0,0); triangles indicate the galaxies found to be members of the clusters. The first quasar (top illustration) is in field number 3 at $z = 0.275$ and at a projected distance of $\sim$1.5 h^{-1} Mpc from the centres of all three central galaxy clusters/subclusters, with estimated redshifts of $z_{\rm est} = 0.28$ for the right and the left subclusters and $z_{\rm est} = 0.30$ for the third cluster in the very centre plus the cluster in the top-right of the image. The second quasar (bottom illustration) is in field number 4 and has redshift $z = 0.194$ and a projected distance to the closest cluster ($z_{\rm est}$ = 0.20) of 1.4 h^{-1} Mpc. The two further clusters seen towards the bottom-left are also at comparable redshifts: $z_{\rm est} = 0.18$ (middle) and $z_{\rm est} = 0.19$ (bottom-left).

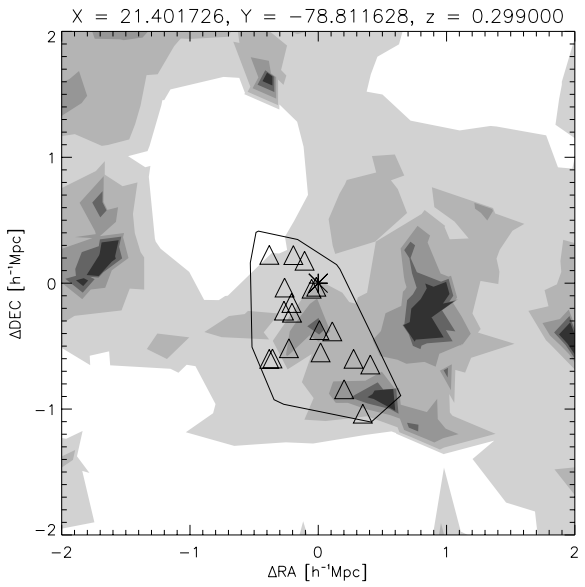

Figure 12. The cluster environment of the quasar (asterisk at coordinates 0,0) in field number 4 and redshift $z = 0.299$, which has the smallest projected distance to the cluster centre. The red galaxies (triangles) have been used to estimate the redshift of the cluster ($z = 0.29$) and determine its boundary (solid line). The density distribution of all galaxies (contours) exhibits prominent peaks (dark areas) outside the galaxy cluster, which demonstrates the importance of the discrimination by colour slicing.

their spectra (Nolan et al. 2001), indicates that interaction/merging processes play the strongest role in the origin and fuelling process of the nuclear activity. The interaction/merging processes include major galaxy mergers, accretion of small gas-rich satellites, tidal interactions between galaxies and the accretion of gas cooling flows. There is a quasar formation and fuelling model based on each of these processes, but the observational assessment of their relative contributions poses a challenge.

Assuming that multiple quasar formation mechanisms coexist, the environments of quasars can give us some clues about their relative contributions. In this study, we find that fewer than 37 per cent of quasars can be found in isolated environments, required by the hot-gas model proposed by Nulsen & Fabian (2000). In this model, quasar formation coincides with formation of an isolated galaxy, where the black hole grows exponentially and is fuelled by the accretion of hot gas during the galaxy formation. This model cannot account for the fact that quasars trace the LSS, because the formation of an isolated galaxy could take place at any location but in the galaxy clusters. The resulting distribution of the quasars with respect to the LSS would correspond to that of random galaxies, which has been found in our investigation to be not the case. There are further arguments against the hot-gas model at least as the only formation mechanism of quasars. In the literature, the majority of the studied host galaxies exhibit morphologies and high luminosities incompatible with newly formed isolated galaxies. Furthermore the model fails to produce high-luminosity quasars at $z \gtrsim 2$, mainly because of the time needed for the black holes to grow (Nulsen & Fabian 2000). Also, it overproduces quasars compared with the observed luminosity function but it reproduces the X-ray background, thus requiring that $\sim$90 per cent of quasars are obscured (Nulsen & Fabian 2000). We have tested if the isolated environment could be an artefact of the magnitude/quality limitations of our data. Reinvestigation of the environments of four quasars using SDSS data has shown, in all four cases, close galaxy clusters which had not been detected in the SSS data. This result makes the hot-gas model, in its original form, a rather unlikely source of low-z quasars, but does not exclude its increasing importance at higher redshifts.

About 20 per cent of the investigated quasars inhabit regions between two possibly merging clusters. As outlined in the previous

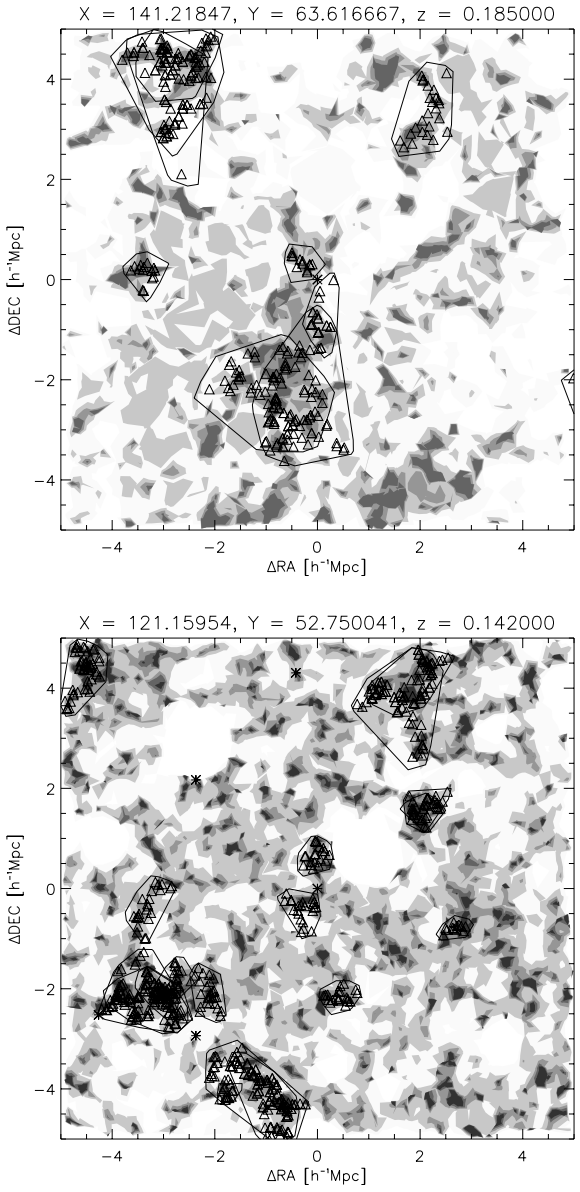

Figure 13. Two examples of quasars found between multiple possibly merging clusters. The contours indicate the density of galaxies; the polygons outline the boundaries of galaxy clusters at comparable redshifts to those of the quasars (asterisks at coordinates 0, 0); triangles indicate the galaxies found to be members of the clusters. The first quasar (top illustration) is in field number 1, has $z = 0.185$ and resides between two clusters at estimated redshifts of $z_{\rm est} = 0.17$ (top) and $z_{\rm est} = 0.22$ (bottom). The second quasar (bottom illustration) is in field number 3, has redshift $z = 0.142$ and resides between two clusters at estimated redshifts of $z_{\rm est} = 0.11$ (top) and $z_{\rm est} = 0.11$ (bottom).

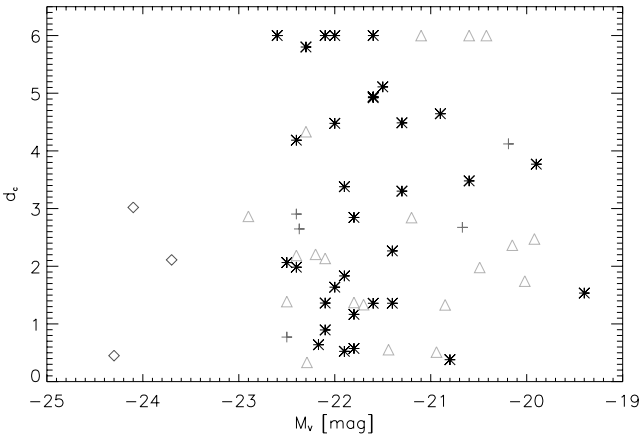

Figure 14. The projected distance $d_{\rm c}$ of quasars to the cluster centres, in units of h^{-1} Mpc, as a function of absolute magnitude M_V. The higher-luminosity quasars ($M_V < -23.0$) are indicated by diamonds, Seyfert 1s by asterisks and 2s by plus symbols. Seyferts without exact spectral classification are indicated by triangles.

section, we can conclude that most, or perhaps even all, quasars found within 1 h^{-1} Mpc of the cluster centre have been formed at the confluence of a cluster merger. Söchting et al. (2002) proposed that the environment of merging clusters could enable quasars to form in galaxy–gas interactions, a mechanism which can be considered as a derivative of the hot-gas model with the difference that the hot gas is not accreted into the protogalaxy but into a cluster galaxy under the influence of the cluster merger.

There are further models, for which at least some of their environmental predictions are met in a cluster merger. Kauffmann & Haehnelt (2000) proposed major mergers as a formation mechanism. This model predicts that quasars form in major mergers of galaxies of similar mass, thus linking quasar formation with spheroid formation. The mergers form supermassive black holes from coalescence of pre-existing black holes, and gas is driven inwards to fuel them. In the very dense environment of merging clusters, the probability of a galaxy–galaxy collision would increase, but the high relative velocities would reduce the efficiency of the galaxies merging. Nevertheless, one of the most luminous quasars in our sample (J101454.9+003337, also quoted in the literature as J1028+0008), which has been found in a cluster-merger environment, has been reported to have a very large elliptical host galaxy with strong indications of a major galaxy merger (McLure et al. 1999). Because we are dealing with a single object, no definite conclusions can be drawn about the relative importance of major mergers as a quasar formation mechanism in the very rich environments of merging clusters. The major-merger model predicts a very massive elliptical host galaxy, but fainter quasars are found in spiral as well as elliptical hosts (McLure et al. 1999), which suggests that the major-merger model is appropriate for luminous quasars, but not for Seyferts and other low-level AGN (Kauffmann & Haehnelt 2002). The major-merger model has been discounted as the only formation mechanism by some other authors. Cattaneo (2001) finds that the single mechanism of major mergers cannot explain the decline of quasar density with epoch and cannot account for the brightest quasars, and consequently supports fuelling by hot gas as a further mechanism of formation. Lake, Katz & Moore (1998) also point out that the lack of association of high quasar luminosity with high host-galaxy luminosity is evidence against the preponderance of major mergers. Nevertheless, the last argument is challenged by the findings of Hamilton, Casertano & Turnshek (2002) that quasar host galaxies span a narrow range of luminosities and are exceptionally bright, much more so than normal galaxies.

Lake et al. (1998) propose that quasars arise from galaxy harassment, in which quasars in low-luminosity host galaxies are fuelled because of harassment by other galaxies in rich cluster environments. Galaxy harassment occurs in clusters where the impact velocities of the galaxies are too high for merging. Their modelling assumes Coma-like clusters, which, of course, are not typical, and it does not incorporate star formation, which is an alternative to active

Table 4. The details of the 60 quasars comprising the sample used for investigation of the cluster environments of quasars. The ΔRA and ΔDec. coordinates mark the position of the quasar in Fig. 10; d_c is the distance of the quasar to the centre of the closest galaxy cluster at comparable redshift. The merging clusters column contains a flag (plus) if the quasar reside between two close galaxy clusters.

Field no.	RA (J2000) (^{h}: ^{m}: ^{s})	Dec. (J2000) ($^\circ$: $'$: $''$)	ΔRA (arcmin)	ΔDec. (arcmin)	z	V	M_V	d_c	Merging clusters
1	09:53:41.5	−00:08:24	−177.1	21.6	0.284	19.99	−21.3	4.49	
1	09:54:36.9	−02:54:44	−163.1	−144.7	0.272	19.19	−22.0	>5	
1	09:56:30.7	−00:34:38	−134.8	−4.6	0.269	19.56	−21.6	4.94	
1	09:57:01.0	−00:42:11	−127.2	−12.2	0.270	19.83	−21.3	3.3	
1	09:57:24.4	−01:19:57	−121.4	−50.0	0.275	20.55	−20.6	3.48	
1	09:58:59.7	+00:47:17	−97.6	77.3	0.236	18.98	−21.9	1.83	
1	10:03:46.0	−02:50:44	−26.0	−140.7	0.218	19.07	−21.6	4.92	
1	10:05:38.5	−01:26:09	2.1	−56.2	0.269	20.33	−20.8	0.38	+
1	10:10:44.4	+00:43:31	76.6	75.5	0.180	16.50	−23.7	2.11	
1	10:11:21.2	−02:12:39	87.7	−102.7	0.204	18.40	−22.1	1.36	+
1	10:12:00.3	−00:09:10	97.6	20.8	0.273	19.25	−21.9	0.52	+
1	10:13:12.1	+02:04:15	115.4	154.2	0.222	17.80	−22.9	2.87	
1	10:13:17.2	−01:10:57	116.8	−41.0	0.202	18.30	−22.2	2.21	
1	10:14:54.9	+00:33:37	141.2	63.6	0.185	15.59	−24.3	0.45	+
1	10:16:57.0	−01:56:15	171.7	−86.3	0.263	19.60	−21.5	>5	
1	10:18:04.4	+00:20:59	188.6	51.0	0.278	18.93	−22.3	>5	
1	10:18:57.7	−01:40:48	201.8	−70.8	0.267	20.17	−20.9	4.64	
1	10:19:11.4	+01:53:54	205.2	143.9	0.190	18.50	−21.8	2.85	
2	00:23:55.7	−31:03:34	−0.9	−3.6	0.215	20.75	−19.9	3.77	
2	00:28:50.8	−30:29:49	62.6	30.2	0.284	19.39	−21.9	3.38	
2	00:29:37.3	−31:02:09	72.3	−2.2	0.145	17.24	−22.5	2.06	
2	00:30:04.3	−28:42:25	79.9	137.6	0.279	17.10	−24.1	3.02	
2	00:35:48.5	−28:29:05	155.7	150.9	0.232	19.23	−21.6	1.36	
2	00:38:50.7	−31:19:51	190.2	−19.9	0.255	19.17	−21.8	1.17	+
2	00:41:05.4	−31:09:03	219.4	−9.1	0.221	18.31	−22.4	1.98	
2	00:40:52.4	−29:02:15	221.3	117.7	0.265	18.49	−22.6	>5	
2	00:44:46.0	−27:14:04	277.0	225.9	0.287	19.66	−21.6	>5	
2	00:45:22.2	−28:58:59	280.4	121.0	0.206	19.18	−21.4	2.27	
2	00:45:29.8	−29:25:53	280.8	94.1	0.179	20.83	−19.4	1.54	
2	00:46:48.8	−29:34:59	297.6	85.0	0.207	18.12	−22.4	2.91	
3	21:20:05.0	−46:01:38	−113.7	−91.6	0.297	19.08	−22.2	0.64	
3	21:26:44.0	−42:43:33	−47.0	106.4	0.141	19.49	−20.2	2.37	
3	21:28:38.7	−45:03:11	−25.0	−33.1	0.242	20.62	−20.2	4.12	
3	21:31:22.4	−46:20:10	3.9	−110.2	0.153	17.44	−22.4	2.65	
3	21:31:39.9	−45:23:48	7.0	−53.8	0.204	19.77	−20.7	2.67	
3	21:33:02.8	−45:48:49	21.4	−78.8	0.299	18.97	−22.3	0.33	
3	21:36:10.4	−46:51:42	53.1	−141.7	0.244	19.38	−21.4	0.55	+
3	21:38:12.5	−44:02:56	77.7	27.1	0.285	20.67	−20.5	1.98	+
3	21:39:44.4	−42:34:23	96.5	115.6	0.168	20.10	−19.9	2.47	
3	21:40:00.6	−44:07:10	97.0	22.8	0.275	20.23	−20.9	1.33	
3	21:39:52.9	−43:15:10	97.0	74.8	0.250	18.38	−22.5	0.77	
3	21:40:41.2	−44:36:10	103.5	−6.2	0.136	19.54	−20.0	1.74	
3	21:41:38.1	−42:53:24	116.9	96.6	0.255	20.50	−20.4	>5	
3	21:42:09.5	−43:37:15	121.2	52.8	0.142	18.71	−20.9	0.51	+
4	02:44:26.3	−01:21:07	−143.4	−111.1	0.201	19.10	−21.7	1.33	+
4	02:46:01.2	−00:59:38	−119.7	−89.6	0.201	18.29	−21.8	1.37	+
4	02:50:03.1	+01:09:28	−59.2	39.5	0.193	18.60	−21.8	0.57	+
4	02:50:07.1	+00:25:29	−58.2	−4.5	0.194	17.61	−22.5	1.39	
4	02:50:25.1	+02:26:59	−53.7	117.0	0.198	18.36	−22.1	2.14	
4	02:51:04.7	+01:19:28	−43.8	49.5	0.231	18.02	−22.1	0.90	+
4	02:51:26.8	+01:15:08	−38.3	45.1	0.300	18.87	−22.0	1.64	+
4	02:52:20.8	+00:43:31	−24.8	13.5	0.175	19.00	−21.2	2.84	
4	02:55:33.8	+01:31:05	23.4	61.1	0.141	16.75	−22.4	2.19	
4	02:56:46.9	+01:13:48	41.7	43.8	0.177	18.20	−22.0	4.48	
4	02:57:55.8	+01:44:36	58.9	74.6	0.282	18.48	−22.4	4.19	
4	02:59:10.8	+00:55:04	77.7	25.1	0.199	19.16	−20.6	>5	
4	02:59:38.2	+00:42:16	84.5	12.3	0.197	18.10	−22.3	4.33	
4	02:59:50.7	+01:03:04	87.7	33.1	0.257	18.90	−22.1	>5	
4	03:00:31.3	+00:53:58	97.8	24.0	0.198	18.87	−21.1	>5	
4	03:01:39.3	+01:45:01	114.8	75.0	0.184	18.54	−21.4	1.36	

Table 5. Number of quasars as a function of projected distance to the cluster centre.

	Projected distance to the cluster centre				
	$<1\ h^{-1}$ Mpc	1–2 h^{-1} Mpc	2–3 h^{-1} Mpc	$>3\ h^{-1}$ Mpc	Cluster mergers
Number of quasars	10	14	14	22	12
Percentage of quasars	16.7 per cent	23.3 per cent	23.3 per cent	36.7 per cent	20 per cent

nuclei for the consumption of gas. Lake et al. imply that harassment might lead to quasars being preferentially located in the outer parts of clusters, which is clearly of relevance to our result that quasars tend to prefer the peripheries. The predictions of this model are best satisfied on the cluster periphery (1–3 h^{-1} Mpc), with cluster mergers not being excluded as a possible site. Around 47 per cent of the quasars in our sample occupy the cluster peripheries, giving some estimate of the relative significance that the galaxy harassment model could have for quasar formation at low redshifts.

These results put the studies of the richness of the quasar environments in a new light, showing that quasars found in rich environments could have formed in cluster mergers whereas those in poorer environments could have been triggered by the infall towards a galaxy cluster. Depending on the distances and masses of the closest galaxy clusters, the richness of the environments of quasars would be expected to exhibit strong variations, making quasars, on small scales, poor tracers of the mass peaks. Results from the literature place quasars in environments with a very wide range of richness (see the introductory section), giving indirect but strong support for our results. We have detected no relation between the optical luminosity of a quasar and its projected distance to the centre of the closest galaxy cluster, which leads to the same conclusion as the richness studies (Finn, Impey & Hooper 2001), that there is no correlation between the density of the environment and the optical luminosity of quasars.

We have shown that low-z quasars are very good tracers of the LSS in galaxy clusters on scales of superclusters. The spatial distribution of the quasar groupings clearly outlines the spatial extent of the underlying superclusters.

The above results, showing that quasars follow a narrow channel of width $\sim 10\,h^{-1}$ Mpc around the LSS in clusters, have the potential, if they apply to quasars at higher redshifts, to explain the clustering on scales $\lesssim 10\ h^{-1}$ Mpc found by Croom et al. (2001b), Shanks & Boyle (1994), Shanks, Boyle & Peterson (1988) and Shanks et al. (1987). This clustering has often been described in terms of an excess of quasar pairs compared with a random distribution. Given that the LSS in clusters is clearly filamentary, and that the quasars are constrained to follow it, the spatial distribution of quasars, when analysed with the isotropic two-point correlation function, will reveal the characteristic $\sim 10\ h^{-1}$ Mpc width of the channel. Thus, this small-scale clustering is, as has been suspected for many years, likely to be also an (indirect) indicator of the mechanisms of quasar formation.

We should emphasize that the quasars in our sample have $z < 0.3$ and are predominantly of low luminosity. We can expect that the relative frequency of the different environments and the dominant mechanisms of formation will be functions of both luminosity and redshift. Most of the objects in our sample are in the luminosity range of Seyfert galaxies, presumably involving mainly spiral hosts, whereas samples at higher redshifts will be of higher luminosity, presumably involving mainly elliptical hosts. Thus, we cannot necessarily extrapolate our results on the relative frequencies of cluster-periphery and cluster-merger-like environments to substantially higher redshifts, although, from the few cases of appropriately wide-field and ultra-deep imaging, there certainly are some qualitative similarities (e.g. the quasar at $z = 1.226$ discussed by Haines et al. 2001). Given that luminous quasars are found almost exclusively in elliptical hosts (McLure et al. 1999) and that ellipticals occupy denser environments (the morphology–density relation; Dressler 1980), we might anticipate an increasing importance of cluster-merger-like environments at higher redshifts.

Future work will include testing our conclusions by studying the morphologies of the host galaxies as a function of their galaxy cluster environment. This additional information may enable us to establish the preferred formation mechanisms on the cluster periphery and at the confluence of cluster mergers. The determination of the evolution of the cluster environment with redshift will allow us to derive the evolution with redshift of the relative importance of the different quasar formation mechanisms to $z \sim 0.8$, which is the redshift limit of our cluster sample found in the Faint Sky Variability Survey (Groot et al. 2003) using the method described here.

If the Great Wall is to some extent a local counterpart of the LSS observed at $z \sim 0.3$, we may assume that the AGN that trace the Great Wall are quasars in their final stages that were formed by mechanisms connected to the environment of its superclusters. If the AGN that trace the Great Wall are not biased (for example, are selected by their X-ray emission) then their morphology should give us information about the host galaxies of the $z \sim 0.3$ quasars. A predominance of low-luminosity disc galaxies would argue in favour of the dominance of the galaxy harassment mechanism for the formation of $z \sim 0.3$ quasars.

ACKNOWLEDGMENTS

We would like to thank the referee, Dr Marek Kukula, for suggesting some helpful clarifications. IKS was funded by a bursary of the University of Central Lancashire UK and by a Marie Curie Fellowship, Improving Human Potential, contract HPMD-CT-2000-00005. The study was carried out using data from the SSS and partly from the SDSS. This research has made use of the SIMBAD data base and the VizieR catalogue access tool, operated at CDS, Strasbourg, France.

REFERENCES

Allard D., Fraley C., 1997, JASA, 92, 1485
Bahcall J. N., Kirhakos S., Saxe D. H., Schneider D. P., 1997, ApJ, 479, 642
Boyce P. J. et al., 1998, MNRAS, 298, 121
Carballo R., Sánchez S. F., González-Serrano J. I., Benn C. R., Vigotti M., 1998, AJ, 115, 1234
Cattaneo A., 2001, MNRAS, 324, 128
Crampton D., Cowley A. P., Hartwick F. D. A., 1989, ApJ, 345, 59
Croom S. M., Smith R. J., Boyle B. J., Shanks T., Loaring N. S., Miller L., Lewis I. J., 2001a, MNRAS, 322, 29
Croom S. M., Shanks T., Boyle B. J., Smith R. J., Miller L., Loaring N. S., Hoyle F., 2001b, MNRAS, 325, 483
Disney M. et al., 1995, Nat, 376, 15
Dressler A., 1980, ApJ, 236, 351

Efstathiou G., Rees M. J., 1988, MNRAS, 230, 5
Ellingson E., Yee H. K. C., Green R. F., 1991, ApJ, 371, 49
Evrard A. E., 1991, MNRAS, 248, L8
Finn R. A., Impey C. D., Hooper E. J., 2001, ApJ, 557, 578
Fukugita M., Shimasaku K., Ichikawa T., 1995, PASP, 107, 945
Girardi M., Borgani S., Giuricin G., Mardirossian F., Mezzetti M., 2000, ApJ, 530, 62
Gladders M., Yee H. K. C., 2000, AJ, 120, 2148
Graham M. J., 1997, PhD Thesis, University of Central Lancashire
Groot P. J. et al., 2003, MNRAS, 339, 427
Haines C. P., Clowes R. G., Campusano L. E., Adamson A. J., 2001, MNRAS, 323, 688
Hambly N. C. et al., 2001, MNRAS, 326, 1279
Hamilton T. S., Casertano S., Turnshek D. A., 2002, ApJ, 576, 61
Hutchings J. B., Crampton D., Morris S. L., Durand D., Steinbring E., 1999, ApJ, 117, 1109
Kauffmann G., Haehnelt M., 2000, MNRAS, 311, 576
Kauffmann G., Haehnelt M., 2002, MNRAS, 332, 529
Kim R. S. J. et al., 2002, AJ, 123, 20
Kodama T., Arimoto N., Barger A. J., Aragón-Salamanca A., 1998, A&A, 334, 99
Kruskal J. B., 1956, Proc. Am. Math. Soc., 7, 48
Lake G., Katz N., Moore B., 1998, ApJ, 495, 152
Lim J., Ho P. T. P., 1999, ApJ, 510, L7
McLure R. J., Dunlop J. S., 2001, MNRAS, 321, 515
McLure R. J., Kukula M. J., Dunlop J. S., Baum S. A., O'Dea C. P., Hughes D. H., 1999, MNRAS, 308, 377
Nolan L. A., Dunlop J. S., Kukula M. J., Hughes D. H., Boroson T., Jimenez R., 2001, MNRAS, 323, 385
Nulsen P. E. J., Fabian A. C., 2000, MNRAS, 311, 346
Okabe A., Boots B., Sugihara K., Chiu S. N., 2000, Spatial Tessellations, 2nd edn. Wiley, New York
Pearson C. P., Rowan-Robinson M., McHardy I. M., Jones L. R., Mason K. O., 1997, MNRAS, 288, 273
Prim R. C., 1957, Bell Syst. Tech. J., 36, 1389
Ramella M., Boschin W., Fadda D., Nonino M., 2001, A&A, 308, 776
Robertson J. G., 1983, PASAu, 5, 144
Sánchez S. F., Gomzáles-Serrano J. L., 1999, A&A, 352, 383
Saxton R. D., Hall P. B., Turner M. J. L., 1999, in Giuricin G., Mezzetti M., Salucci P., eds, ASP Conf Ser. Vol. 176, Observational Cosmology: The Development of Galaxy Systems. Astron. Soc. Pac., San Francisco, p. 389
Shanks T., Boyle B. J., 1994, MNRAS, 271, 753
Shanks T., Fong R., Boyle B. J., Peterson B. A., 1987, MNRAS, 227, 739
Shanks T., Boyle B. J., Peterson B. A., 1988, in Osmer P., Porter A. C., Green R. F., Foltz C. B., eds, ASP Conf. Ser. Vol. 2, Optical Surveys for Quasars. Astron. Soc. Pac., San Francisco, p. 244
Söchting I. K., Clowes R. G., Campusano L. E., 2001, in Clowes R., Adamson A., Bromage G., eds, ASP Conf. Ser. Vol. 232, The New Era of Wide Field Astronomy. Astron. Soc. Pac., San Francisco, p. 123
Söchting I. K., Clowes R. G., Campusano L. E., 2002, MNRAS, 331, 569
Stoughton C. et al., 2002, AJ, 123, 485
Teplitz H. I., McLean I. S., Malkan M. N., 1999, ApJ, 520, 469
Véron-Cetty M. P., Véron P., 2001, A&A, 374, 92
Wold M., Lacy M., Lilje P. B., Serjeant S., 2001, MNRAS, 323, 231
Yee H. K. C., 1992, in Fabian A. C., ed., Clusters and Superclusters of Galaxies. Kluwer, Dordrecht, p. 293
Yee H. K. C., Green R. F., 1987, ApJ, 319, 28

This paper has been typeset from a TEX/LATEX file prepared by the author.